



VICTORIA UNIVERSITY
MELBOURNE AUSTRALIA

Quantitative study of Artemisia pollens deposition in the upper airways of children with adenoidal hypertrophy

This is the Accepted version of the following publication

Hu, Zhenzhen, Ma, Ruiping, Wang, Yusheng, Lou, Miao, Gong, Minjie, Wang, Botao, Zheng, Guoxi, Dong, Jingliang and Zhang, Ya (2023) Quantitative study of Artemisia pollens deposition in the upper airways of children with adenoidal hypertrophy. *Journal of Aerosol Science*, 172. ISSN 0021-8502 (In Press)

The publisher's official version can be found at
<https://www.sciencedirect.com/science/article/pii/S0021850223000563?via%3Dihub>
Note that access to this version may require subscription.

Downloaded from VU Research Repository <https://vuir.vu.edu.au/45851/>

Quantitative study of *Artemisia* pollens deposition in the upper airways of children with adenoidal hypertrophy

Zhenzhen Hu ^{a,1}, Ruiping Ma ^{a,1}, Yusheng Wang ^a, Miao Lou ^a, Minjie Gong ^a,
Botao Wang ^a, Guoxi Zheng ^a, Jingliang Dong ^{b,c,**}, Ya Zhang ^{a,*}

^a Department of Otolaryngology Head and Neck Surgery, The Second Affiliated Hospital of Xi'an Jiaotong University, Xi'an, Shaanxi, 710004, China

^b Institute for Sustainable Industries & Liveable Cities, Victoria University, Footscray, VIC 3011, Australia

^c School of Engineering, RMIT University, Bundoora, VIC, 3083, Australia

* Corresponding author. Department of Otolaryngology Head and Neck Surgery, The Second Affiliated Hospital of Xi'an Jiaotong University, 157 Xiwu Road, Xi'an, Shaanxi, 710004, China.

** Corresponding author.

E-mail addresses: jingliang.dong@vu.edu.au (J. Dong), zhangya@xjtu.edu.cn (Y. Zhang).

¹ Authors contributed equally as first authors.

ABSTRACT

Studies regarding the pollen transport and deposition in children nasal airways are still scarce, especially the regional deposition doses, which is difficult to provide guidance for precise application of pollen blockers and nasal administration. In addition, most previous investigations included only one child case, which lacked statistical significance. To this end, we used computational fluid particle dynamics (CFPD) modeling approach to calculate the deposition pattern of *Artemisia* pollen at various anatomical sites in the upper airway of 12 children with adenoid hypertrophy (AH), and analyzed the effects of respiratory flow rate and pollen density on the deposition distribution. Adult nasal airways from our previous study were included for data comparison. We found that nasal cavities of children with AH aged 4-6 years had a greater area/volume ratio than adults did, and the area and volume of the turbinate region were less than half that of adults. The physical diameter of *Artemisia* pollen was set to 21.0 μm , with a shape of ellipsoid. Its average density is 1080 kg/m^3 in the humid state and 550 kg/m^3 in the dry state. In resting state, children with AH had higher deposition rates of wet *Artemisia* pollen in the nasal septum and nasopharynx, and lower deposition rates in the nasal vestibule and middle turbinate compared with adults. Under exercising conditions, wet pollen was deposited mainly in the nasal vestibule and the anterior part of the nasal septum in children. Compared to wet pollen, the deposition rate of dry *Artemisia* pollen in resting state was approximately halved and the pollen entering the lower respiratory tract rose approximately 47-fold. The findings suggest that nasal cavities of children are not simply scaled-down version of adults. Notable differences in deposition hotspots and deposition patterns have been discovered between the two. The deposition hotspots shifted significantly forward as the respiratory flow rate increased. Dry *Artemisia* pollen has a low density and is more likely to enter the lower respiratory airways, which may put children at a higher risk of developing asthma.

Keywords: Pollen, Computational fluid particle dynamics, Particle deposition, Nasal cavity, Adenoid hypertrophy.

1. Introduction

Adenoid hypertrophy (AH) affects 42-70% of children and adolescents, and the sizes of adenoids typically

peak between the ages of 2 and 6 years, after which the adenoid tissue would degenerate (Pereira et al., 2018; Evcimik et al., 2015). AH is one of the most common causes of upper airway obstruction and obstructive sleep apnea (OSA) in children (Marcus et al., 2012). The presence of allergic rhinitis (AR) has been demonstrated to be a risk factor for AH in children, and children with allergic diseases have a greater chance to develop AH than those without allergic diseases (Evcimik et al., 2015; Modrzynski & Zawisza, 2007a). In turn, the presence of AH increases the severity of AR and prolongs the course of the disease (Dogru et al., 2017). Therefore, some researchers have hypothesized that children with both AR and AH may be sensitive to specific allergens (Modrzynski & Zawisza, 2007b; Huang & Giannoni, 2001). For example, Huang and Giannoni (2001) showed that children with both AR and AH are more likely to be allergic to pollen allergens. As one of the dominant outdoor allergens during summer and autumn in northwest China, Artemisia pollen, characterized by its large quantity, small size, and strong allergenicity, is a major carrier of airborne toxins (Zhang et al., 2019). It is anticipated that a better understanding of the deposition pattern of pollen allergens in various anatomical sites in the nasal cavity of children with AH may shed light on the mutual causative pathogenesis between AH and AR.

However, due to the complex geometry of the nasal cavity, traditional experimental approaches are difficult to quantify the local flow field and particle deposition rates in the nasal cavity. In contrast, computational fluid dynamics (CFD) has the advantage of providing thorough information on airflow and aerosol deposition that is more pertinent to health outcomes. To date, the majority of CFD studies on aerosol deposition have focused on the nasal cavities of adults, while few studies on particle deposition in the nasal cavity of children have been reported. The work of Zhang et al. (2019), Inthavong et al. (2021), Tian et al. (2019), Hazeri et al. (2021), Dong et al. (2019), Garcia et al. (2015), and Farhadi et al. (2012) present the recent study of aerosol and nano/micro-particle deposition in the adult nasal cavity. Dong et al. (2022) evaluated inspiratory airflow patterns in human nasal cavities with wide age difference, including child, adult and elderly people, and Moredu et al. (2019) evaluated nasal congestion symptoms in children, both of them did not study particle deposition. Only Xi et al. (2011) studied the nasal aerosol deposition in a 5-year-old child and discovered significant variations in the deposition of inhaled aerosols between children and adults. Later, Xi et al. (2014a) investigated the dynamics of inhaled aerosols in 4 cases of children (10-day-old, 7-month-old, 3- and 5-year-old) and compared them with an adult and found that age could significantly affect the deposition of micron particles. In the same year, Xi et al. (2014b) studied the impact of facial interface on micron particle inhalation and deposition in a healthy child airway model and found that more realistic inhalation exposure conditions led to appreciable changes in airflow dynamics and aerosol inhalation near the nostrils. Recently, Sun et al. (2022) studied the transport and deposition of nanoparticles in the nasal cavity of a 3-year-old child with AH. The majority of these previous investigations only included one case of children, which lacks statistical significance. Moreover, there is a dearth of data regarding particle deposition in various anatomical regions within the nasal cavity of children. Without a clear understanding of the areas where pollen deposition is most concentrated, physicians may find it challenging to offer precise advice on the use of pollen blockers and nasal drug delivery.

This study enrolled the largest cohort of subjects to date, which included anatomically accurate upper airway models in 12 children with AH. We quantified the geometric characteristics of the nasal cavity of children aged 4-6 years and analyzed the flow field characteristics of each anatomical site in detail. For the first time, a database of Artemisia pollen deposition in each anatomical site of the upper airway of children with AH was constructed, which provides a reference for accurate prevention and precise medication of hay fever in children with AH.

2. Methods

2.1. Study subjects

Twelve Asian children (6 males and 6 females, aged 5 ± 0.83 years) diagnosed with AH by computed

tomography (CT) examination were collected. The adenoidal/nasopharyngeal (A/N) ratio is defined as the ratio of the adenoid thickness to the nasopharyngeal width, which reflects the adenoid size and nasopharyngeal airway patency (Fujioka et al., 1979). The specific measurement of the A/N ratio can be found in Moideen et al. (2019). In this study, the method of calculating the AN ratio based on CT images is shown in Fig. 1. The A/N ratio of normal children was 0.583 ± 0.0741 (Elwany, 1987). The A/N ratio of all the children in this study was 0.80 ± 0.082 . The children had no significant abnormalities in nasal anatomy and morphology and no previous history of severe sinusitis, nasal malformation, nasal septal perforation, nasal tumor, or nasal surgery history. The parents of the children all signed a written informed consent form and are fully aware of the relevant facts and risks involved, and the study was approved by the Institutional Review Board and Medical Ethics Committee of the Second Affiliated Hospital of Xi'an Jiaotong University (2021-186).

2.2. Computed tomography (CT) scan

The Siemens Dual Source photon CT Machine was used to perform nasal scans, which is characterized by low radiation dose and fast scanning speed. The radiation dose range of children's CT examination in this study was 2.81 to 5.10mGy, consistent with the radiation dose range (1.13 - 6.11mSv) of children's head CT in the study of Simantirakis et al. (2011). The CT scans included coronal, axial and sagittal images with a resolution of 512×512 pixels and a slice interval of 0.5 mm, covering the upper airway region. CT images were obtained in Digital Imaging and Communications in Medicine (DICOM) format.

2.3. 3D modeling and numerical simulation

Images in DICOM format were imported into Mimics software for the reconstruction of the upper airway (including the nasal cavity, pharynx and larynx) in children. Studies have shown that the existence of facial features significantly affects airflow entering the nostrils (Anthony et al., 2005; Inthavong et al., 2009; Shang et al., 2015). Therefore, in this present study, the geometry of the face was preserved and a hemisphere with a radius of 100 mm was attached in front of the face (Fig. 2A). After completing the reconstruction, the surfaces of the models were smoothed and regional divisions were performed. According to the anatomical location of each region, the upper airway models of the children were divided into the nasal vestibule, nasal atrium, nasal septum, inferior turbinate, middle turbinate, superior turbinate, olfactory, maxillary sinus, nasopharynx and larynx (Fig. 2B). Then, Fluent Meshing was used to generate polyhedral cells with prism layers and 3D computational domain (Fig. 3), which is a new polyhedral mesh generation method with a minimum mesh size of 0.1 mm for the main airway and a maximum mesh size of 8 mm for the external domain. Near wall refinement with 5 layers of prism mesh were created to better resolve the near wall flow and associated particle transport behaviours. The first prism layer was set to 0.02 mm and the growth rate was 1.1. After independent tests with coarse, medium and thin polyhedral meshing density, the final mesh numbers are between 0.8 ~ 1.2 million.

Mouth breathing is possible, but in this study only nasal breathing was considered. The tidal volume and respiratory rate of children were obtained based on published respiratory parameters (Hofmann, 1982). 2.7s was set as one breathing cycle in this study (Thiriet, 2014). The inspiratory flow rates of children aged 4 years, 5 years, and 6 years old subjects in the resting state were calculated to be 9.03, 9.77, and 10.72 L/min, while the inspiratory flow rates were set as 18.06 19.54 and 21.44 L/min under the condition of low-load exercise, respectively. The SST κ - ω model was used to simulate the aerodynamic characteristics of the upper airway in children. The flows in this study were assumed to be incompressible and stable. The out-of-face sphere is defined as the "pressure inlet" and the outlet of the domain is set as the "velocity outlet". The external ambient air temperature was 24 °C and the internal nasal surface was assumed 37 °C. The air density is 1.225 kg/m^3 and the dynamic viscosity coefficient was $1.7894 \times 10^{-5} \text{ kg/ms}$. The incompressible Navier-Stokes equation was

determined to be the control equation, and the Second Order Upwind algorithm was used to calculate the airflow in the nasal cavity during steady-state inhalation.

For a dispersed phase (particles) with low volume fraction, one-way coupled Lagrangian approach was used. In this approach, the airflow field is first simulated, and then the trajectories of individual particles are tracked by integrating the particle force balance equation. For nanoparticles, deposition is mainly influenced by Brownian diffusion. For particles in the micron range larger than 1 μm , deposition by inertial collisions dominates, while the effect of Brownian diffusion is negligible (Inthavong et al., 2009; Dong et al., 2016). In this study, only the gravity and the drag force were considered for tracking the Artemisia pollen particles. The motion of particles in Cartesian coordinates was given as,

$$\frac{du_i^p}{dt} = f_D + f_G \quad (1)$$

where u_i^p is the particle velocity, t is the time, f_G is the force of gravity, f_D is the drag force per unit particle mass taking the form of Stokes' drag law (Ounis et al., 1991) defined as,

$$f_D = \tau_p(u_i^g - u_i^p) \quad (2)$$

where τ_p is the particle response time, u_i^g is the airflow velocity, $\tau_p = 18\mu/d_p^2\rho_p C_c$, and C_c is the Cunningham correction factor to Stokes' drag law, which is calculated from,

$$C_c = 1 + \frac{2\lambda}{d_p} (1.257 + 0.4e^{-(1.1d_p/2\lambda)}) \quad (3)$$

where λ is the air molecular mean free path, and d_p is the particle volume equivalent diameter.

The geometric properties of Artemisia pollen are shown in Table 1 (Crawford, 1949; James & Kurt, 1963; Depciuch et al., 2016). The shape factor is the ratio of the surface area of a sphere having the same volume as the particle to the actual surface area of the particle. In the discrete phase model (DPM), particles were uniformly released in the anterior nostril plane with an initial velocity of 0m/s. The physical diameter of Artemisia pollen was set to 21.0 μm , with a shape of ellipsoid and a shape factor of 0.99. Its average density is 1080 kg/m^3 in the humid state and 550 kg/m^3 in the dry state. Non-spherical drag law was activated to calculate the C_D value for each particle, which is calculated from,

$$C_D = \frac{24}{Re_{sph}} (1 + b_1 Re_{sph}^{b_2}) + \frac{b_3 Re_{sph}}{b_4 + Re_{sph}} \quad (4)$$

where,

$$\begin{aligned} b_1 &= \exp(2.3288 - 6.4581\varphi + 2.4486\varphi^2) \\ b_2 &= 0.0964 + 0.5565\varphi \\ b_3 &= \exp(4.905 - 13.8944\varphi + 18.4222\varphi^2 - 10.2599\varphi^3) \\ b_4 &= \exp(1.4681 + 12.2584\varphi - 20.7322\varphi^2 + 15.8855\varphi^3) \end{aligned}$$

The shape factor, φ , is defined as,

$$\varphi = \frac{s}{S} \quad (5)$$

where s is the surface area of a sphere having the same volume as the particle, and S is the actual surface area of the particle. For the purposes of calculating particle mass, drag force, and Re_{sph} , the particle size d_p should be the diameter of a sphere having the same volume.

Ohsaki et al. (2019) reported that the particle shape had an impact on the particle deposition behavior. The rod-like particles with larger aspect ratio (aspect ratio=4) tend to have higher reachability into the depths of a simple respiratory model. However, in this study, the aspect ratio of Artemisia pollen was found to be 1.07, which is very close to 1, and its shape factor was 0.99, indicating that the shape of Artemisia pollen is nearly spherical, and the orientation of particles may have minimal impact on particle transport and deposition patterns. To confirm the validity of this simplification, we compared the deposition results of wet Artemisia pollen obtained from simulations of model G that considered particle orientation with those that did not. Fig. 4

demonstrates that both simulation approaches yield nearly identical regional deposition results for wet pollen with a physical diameter of 21 μ m. Therefore, particle orientation was not taken into account in this study.

2.4. Statistical methods

Statistical analysis was performed using SPSS 21.0 software. The differences among groups under varied flow rates and densities were compared by paired t-test. $p < 0.05$ was considered statistically significant.

3. Results

3.1. Geometric characteristics

The distance from the tip of the nose to the choana was defined as the length of the nasal cavity, and the distance from the top to the bottom of the nasal cavity was defined as the height of the nasal cavity (Fig. 2B). The nasal cavity volume was measured from the vestibule to the choana (excluding the nasopharynx). The length of the nasal cavity in children aged 4-6 years was (5.59 ± 0.31) cm, and the height was (3.52 ± 0.24) cm. The unilateral surface area of the nasal cavity was (49.77 ± 5.12) cm², the unilateral volume was (5.41 ± 0.98) cm³, and the area/volume was (9.38 ± 1.30) cm⁻¹. The surface area of the unilateral turbinate region was (25.85 ± 3.01) cm² and the volume of the unilateral turbinate region was (2.37 ± 0.64) cm³. The volume of the unilateral turbinate region is the sum of the volume of the inferior, middle, and superior turbinate of the unilateral nasal cavity. The volume of the nasopharynx was (2.13 ± 0.66) cm³ (excluding the larynx).

3.2. Flow field analysis

Although the geometries of the individual models varied from each other (Fig. 5), a general trend in the inhaled airflow can be observed in the children's nasal models. The results of this study are schematically represented by model G. As shown in Fig. 6, airflow went obliquely upward into the nasal cavity from the nostrils, and then the majority became diverted horizontally backward after passing through the nasal valve. After leaving the choana, the airflow turned again and descended vertically into the pharynx. Obvious vortices were formed in the anterosuperior part of the nasal cavity, the anterior part of the inferior turbinate and the larynx, which were caused by the sudden increase of the cross-sectional area, resulting in local airflow separation and counterflow.

To better demonstrate the local airflow, 11 cross-sections perpendicular to the mainstream airflow were set in the nasal cavity and pharynx (Fig. 7). The anterior nostril cross-section was set as Inlet, cross-sections C1-C3 were inside the nasal vestibule and nasal valve area, cross-sections C4-C8 were set in the anterior head of inferior turbinate, anterior head of middle turbinate, middle part of inferior turbinate, the middle part of middle turbinate, and posterior part of the inferior turbinate, and cross-sections C9-C11 were set in the choana and nasopharynx. The direction of the airway from the anterior nostril to the nasal valve area was getting closer to the septum side and the size of the airway lumen gradually narrowed. The eccentrically concentrated main airflow (shown in red) was gradually shifting from the lower inner side of the Inlet section to the outer upper side of the C3 section. In addition, due to the increased section area of the airway from the anterior nostril to the nasal vestibule, vortices were formed and observed in the C1 and C2 planes, suggesting the presence of airflow separation and recirculation. C4 to C8 planes were the turbinate region, where the high flow velocity area was mainly concentrated in the nasal common meatus and middle nasal meatus, but not in the olfactory region and nasal bottom. C6-C7 planes were located at the ostium of the maxillary sinus, where we can see that airflow rarely entered the maxillary sinus. In addition, the cross-sectional area from C6 to C7 further increased and the average velocity started to slow down. C9 to C11 planes were located at the choana and the nasopharynx, respectively, where a clear vortex formation could be observed. The velocity of airflow in this region was

significantly lower than that in the nasal cavity, but the disturbance of airflow was more intense due to the convergence of airflow from both sides of the nasal cavity and the drastic change of the cavity cross-section. After the airflow out-flew the choana, the retropharyngeal wall was scoured and vortexes were formed after the airflow impingement.

3.3. Model evaluation

The impaction parameter ($d_{ae}^2 Q$) has been widely used for determining particle deposition rate by considering both particle sizes and flow rates, where d_{ae} is the aerodynamic equivalent diameter (μm) and Q is the volume flow rate (L/min). To confirm the reliability of the numerical simulations, the deposition fraction results for particle diameters in the range of 1–40 μm were compared with published deposition data on children.

The comparison as a function of impaction parameter ($d_{ae}^2 Q$) was shown in Fig. 8A. The deposition data of our models were compared with the mean (mean \pm standard deviation) of the deposition data of Golshahi et al. (2011). Fig. 8A also shows deposition data in a child's nasal airway replica (Zhou et al., 2013) and in vivo nasal deposition data in children (Becquemin et al., 1991; Bennett et al., 2008). The predicted deposition fraction profile produced an S-shaped inertial curve, and the simulation results were in reasonable agreement with the deposition data of Zhou et al. (2013), Becquemin et al. (1991), Bennett et al. (2008), and Golshahi et al. (2011), considering the intersubject variability, illustrated with the standard deviation. As the impaction parameter increases, the deposition profile increases sharply and reaches complete deposition when impaction parameter is greater than 10,000 $\mu\text{m}^2\cdot\text{L}/\text{min}$.

A parameter that includes the pressure drop (Δp) of a whole model was used to reduce the scatter of deposition data. Fig. 8B shows deposition in our models and the replicas from the Golshahi et al. (2011) and Zhou et al. (2013) study as a function of $d_{ae}^2 \Delta p$. When deposition parameter ranges from 90 to 1,100, the deposition data of the child model in this paper is obviously in better agreement with the data of Golshahi et al. (2011). This pressure parameter does reduce the scatter of deposition data considerably, as also was demonstrated in a follow up study by Golshahi and Hosseini (2019).

3.4. Deposition distribution and trajectory of *Artemisia pollen*

Particle deposition is a process where inhaled particles are "captured" by the nasal mucosa stopping them from moving into the deeper airways. The deposition rate of each site can be calculated by the following formula: Deposition rate = local deposition particle number / total inhaled particle number $\times 100\%$. Escape rate can be calculated by the following equation: Escape rate = number of particles escaping from larynx / total inhaled particle number $\times 100\%$. Fig. 9AB depicts the regional deposition pattern of wet *Artemisia pollen* in the upper airway of the representative subject (model G) with AH in resting state. About $82\% \pm 14.50\%$ of the wet *Artemisia pollen* was deposited in the nasal cavity (except nasopharynx and larynx), and less than 1% of the pollen escaped from the larynx. The most common deposition sites were successively nasal septum ($51.62\% \pm 17.34\%$), nasal vestibule ($19.05\% \pm 8.00\%$), nasopharynx ($13.79\% \pm 13.57\%$), middle turbinate area ($5.11\% \pm 4.9\%$) and larynx ($4.62\% \pm 4.72\%$). The deposition rates were only $3.88\% \pm 3.54\%$ in the inferior turbinate area and $1.30\% \pm 1.50\%$ in the nasal atrium. Additionally, the superior turbinate area and the olfactory both had deposition rates of less than 1%, whereas the maxillary sinus had a deposition rate of less than 0.1% and was nearly particle-free. Detailed model anatomy and deposition data descriptions can be found in Table 2.

The trajectory diagram of wet *Artemisia pollen* as it moved following airflow is shown in Fig. 9CD. Compared with the airflow diagram in Fig. 6, the particle trajectory diverged from the main streamline when the airflow took a steep turn, resulting in particles to strike the nasal wall and produce deposition. The majority of pollen trajectories impacted in the anterior 1/3 of the nasal cavity, and only a small amount of pollen followed the main airflow passing the common nasal tract and entering the nasopharynx, while particle trajectories were

sparse in the middle and inferior turbinate areas.

Our group previously published a study on the deposition of *Artemisia* pollen in the nasal cavity of adults (Zhang et al., 2019). To understand the similarities and differences in particle deposition between children and adults, the deposition rates of nasal *Artemisia* pollen in children with AH were compared with those in healthy adults. The sample size of the adult cohort was 30 healthy Asian adults, and the wall regions in the models were defined using the same anatomical boundaries as the children. Unlike the child model, the adult model did not include the maxillary sinuses and larynx. Detailed model anatomy and deposition data descriptions can be found in Table 3. As shown in Fig. 9E, the wet *Artemisia* pollen deposition rate in the nasal cavity of adults was approximately 77%, and the anatomic sites of adults showing the highest deposition rates were in sequence of the nasal septum ($30.70\% \pm 12.27\%$), nasal vestibule ($27.45\% \pm 8.21\%$), middle turbinate area ($13.59\% \pm 8.98\%$) and nasopharynx ($7.14\% \pm 5.90\%$). Whereas the deposition rate in children's nasopharynx was higher than that in the middle turbinate area. Compared with adults, the deposition rates were significantly higher in the nasal septum and nasopharynx of children with AH ($p < 0.05$), and the deposition rates were significantly lower in the nasal vestibule and middle turbinate region ($p < 0.01$). No significant difference in the deposition rate of the inferior turbinate region ($3.88\% \pm 3.54\%$ vs. $3.30\% \pm 2.90\%$, $p > 0.05$) between the two groups was observed. In addition, the pollen escape rate was significantly lower in children compared to adults ($0.19\% \pm 0.39\%$ vs $17.00\% \pm 9.57\%$, $p < 0.01$).

We also compared the pollen dose deposited in the nasal cavity of children and healthy adults. This dose expressed in the unit of micrograms/cm² considers the different inhalation rates and different sizes of children and adults. The inspiratory flow in normal adults is 15 L/min (Zhang et al., 2019). As shown in Fig. 9F, the deposition doses were significantly higher in the nasal atrium, nasal septum, inferior turbinate region and nasopharynx of children nasal subjects with AH compared to adults ($p < 0.01$). No significant difference in the deposition dose of nasal vestibule, middle turbinate region, superior turbinate region and olfactory region between the two groups was observed ($p > 0.05$). In addition, the pollen escape dose was significantly lower in children compared to adults ($p < 0.05$). Detailed deposition and anatomical data were listed in Table 2 and 3.

3.5. Effect of different inhalation flow rates

The pattern diagram and trajectory diagram of wet *Artemisia* pollen deposition in the exercising state are shown in Fig. 10A-D. With the increase of inspiratory velocity, the secondary flow, turbulent diffusion and particle momentum in nasal cavity were correspondingly increased. Compared with the deposition pattern in Fig. 9AB, pollen was deposited almost entirely in the anterior 1/3 of the nasal cavity including the nasal vestibule and the anterior part of the nasal septum, and almost no particles were deposited in the nasal turbinate region in the deep part of the nasal cavity and in the nasopharynx. Compared with the trajectory diagram in Fig. 9CD, in exercising state, the pollen could hardly follow the main airflow to turn due to the excessive particulate inertia, and the curvature of the trajectory line is relatively flat and straight, therefore most particles directly collided into the nasal cavity wall.

The deposition rates of wet *Artemisia* pollen at each anatomical site at different flow rates are shown in Fig. 10E. Under exercising conditions, the wet pollen deposition rate prominently increases in the nasal vestibule ($24.85\% \pm 8.48\%$ vs. $19.05\% \pm 8.00\%$, $t=11.977$, $p < 0.01$) and the nasal septum ($69.22\% \pm 10.05\%$ vs. $51.62\% \pm 17.34\%$, $t=5.194$, $p < 0.01$) compared to the resting state. That is, about 94% of the pollen was deposited in the anterior 1/3 of the nasal cavity. While the deposition rate in other areas saw a decrease, including the middle turbinate region ($1.25\% \pm 3.15\%$ vs. $5.11\% \pm 4.9\%$, $t=-6.288$, $p=0.000$), olfactory region ($0.04\% \pm 0.13\%$ vs. $0.31\% \pm 0.39\%$, $t=-3.905$, $p=0.001$), nasopharynx ($0.93\% \pm 1.36\%$ vs. $13.79\% \pm 13.57\%$, $t=-5.032$, $p=0.000$) and larynx ($0.05\% \pm 0.12\%$ vs $4.62\% \pm 4.72\%$, $t=-4.756$, $p=0.000$). The escape rate decreased from $0.19\% \pm 0.39\%$ to 0.00% , that is to say, that no pollen escaped into the lower respiratory tract ($t=-2.382$, $p < 0.05$).

3.6. Effect of different pollen densities

The deposition distribution and particle trajectory of dry *Artemisia* pollen in resting state are shown in Fig. 11A-D. In the dry climate, the density of *Artemisia* pollen decreased, resulting in a reduced momentum of its movement in the nasal cavity. Compared with the deposition diagram in Fig. 9AB, the deposition of dry *Artemisia* pollen particles in the nasal cavity is significantly reduced, and the pollen that escaped from the outlet into the deeper airway is significantly increased. Compared with the trajectory diagram in Fig. 9CD, the dry pollen could trace the airflow currents in a longer travel distance compared to wet *Artemisia* pollen, therefore most trajectory lines could pass through the nasopharynx.

As shown in Fig. 11E, the deposition rate of dry *Artemisia* pollen was significantly lower in the nasal vestibule ($11.77\% \pm 6.96\%$ vs $19.05\% \pm 8.00\%$, $t = -9.803$, $p < 0.01$) and the nasal septum ($14.59\% \pm 13.09\%$ vs $51.62\% \pm 17.34\%$, $t = -14.014$, $p < 0.01$) compared to wet *Artemisia* pollen. While the inferior turbinate area ($5.43\% \pm 3.27\%$ vs $3.88\% \pm 3.54\%$, $t = 3.336$, $p = 0.003$), middle turbinate area ($11.89\% \pm 4.18\%$ vs $5.11\% \pm 4.90\%$, $t = 6.494$, $p = 0.000$), nasopharynx ($22.92\% \pm 18.05\%$ vs $13.79\% \pm 13.57\%$, $t = 3.770$, $p = 0.001$) and larynx ($22.35\% \pm 13.90\%$ vs $4.62\% \pm 4.72\%$, $t = 7.950$, $p = 0.000$) had significantly higher deposition rates. Meanwhile, the maxillary sinus saw a slightly elevated deposition rate ($0.08\% \pm 0.15\%$ vs $0.01\% \pm 0.02\%$, $t = 2.259$, $p = 0.034$). In addition, the escape rate of pollen increased from $0.19\% \pm 0.39\%$ to $8.90\% \pm 11.55\%$, showing a surprisingly 47-fold increase ($t = 3.774$, $p < 0.01$).

3.7. Transport time of inhaled pollen particles

We counted the travel time of inhaled pollen particles from the anterior nostril to the outlet of the larynx in 12 child models. The average transport time of inhaled wet pollen particles was 0.45s, and the transport time of one pollen particle with the longest transport time was 1.14s. The average transport time of inhaled dry pollen particles was 9.47s, and the transport time of one pollen particle with the longest transport time was 42.23s. Due to the difference in initial density between dry and wet pollen, dry pollen has a lower density, which increases the likelihood of dry particles being trapped and carried along with the airflow vortex due to the occurrence of airflow separation in the upper anterior section of the nasal cavity, so the residence time is significantly increased. The movement trajectory of inhaled pollen particles over time is shown in Fig. 12.

4. Discussion

Particle deposition in the human nasal cavity is caused by four different deposition mechanisms: inertial impaction, sedimentation, diffusion and interception (Wang et al., 2009). Shang et al. (2015) concluded that nasal vestibule, nasopharynx and middle turbinate region are the three highly concentrated deposition hotspots for micron particles to deposited in the nasal cavity. Wet *Artemisia* pollen deposited mostly in the nasal septum among children with AH, which is also the primary site for concomitant nasal itching symptoms among AR children. Next, nasal vestibule, nasopharynx and middle turbinate area, respectively, were the next most common locations for *Artemisia* pollen to deposit in this paper, which well aligns with Shang et al. (2015).

Zhang et al. (2019) and Xi et al. (2014) reported that the unilateral nasal mucosa has an average area of $(89.7 \pm 8.9) \text{ cm}^2$, an average volume of $(11.2 \pm 1.9) \text{ cm}^3$, and area/volume of $(8.2 \pm 1.5) \text{ cm}^{-1}$, while the mucosal area of bilateral turbinate area was 112.59 cm^2 , and the volume was 12.63 cm^3 . The nasal mucosa of children aged 4-6 years in this study had an area and volume that were roughly half that of adults, while the area/volume ratio was higher than that of adults. The surface area of the turbinate area of children was only 38% of that of adults and the volume was 46% of that of adults. These indicate that the anatomy of the nasal cavity in children

1 is quite unique and definitely not a simple scaling-down of the adult nasal cavity. The children's nasal cavities
2 feature smaller volumes but larger mucosal surface area per unit volume compared with adults, which makes
3 it simpler for particles to deposit when passing through. Multiple clinical studies have found that the proportion
4 of children with moderate/severe AR is significantly higher than that of adults ([Izquierdo-Dominguez et al.,](#)
5 [2013](#); [Izquierdo-Dominguez et al., 2017](#)). From the standpoint of particle deposition, this clinical phenomenon
6 may be related to a higher rate of total pollen deposition in the nasal cavities of children than in adults.
7 Deposition rates in the nasal vestibule and middle turbinate area were significantly lower in children with AH
8 compared to adults, whereas deposition rates in the nasal septum and nasopharynx were significantly higher.
9 The low deposition rate of the nasal vestibule may be due to the shorter length of the nasal vestibule in children
10 contributed to shorter interception time of particles. The low deposition rate in the middle turbinate area and
11 the high deposition rate in the nasal septum are due to the fact that the turbinate in children is still in the
12 developing stage, especially the middle turbinate, which is small in size and thin in bone substance and
13 submucosal tissue. The high deposition rate in the nasopharynx can be attributed to the obstruction of the
14 choana by hypertrophic adenoids, which leads to the increased impact of airflow on the posterior pharyngeal
15 wall, and more pollen particles are deposited in the nasopharynx by direct collision. [Lou \(2018\)](#) also mentioned
16 that AH may lead to accumulation of allergens (such as dust and pollen) in the nasal cavity and nasopharynx,
17 thereby exacerbating AR symptoms and duration.

21 We also observed the overall regional deposition dose profile well aligned with the airflow patterns, where
22 airflow mainly passed through the lower and middle part of the main nasal passage after passing the nasal
23 vestibule, whereas the airflow in nasal turbinate region seemed sparse. This airflow pattern resulted in high
24 deposition dose in the nasal septum and significantly low deposition doses in the upper, middle and lower
25 turbinate regions. The deposition dose per unit area in the nasal septum, inferior turbinate region and
26 nasopharynx is significantly higher in children with AH compared to adults, mainly due to the fact that the
27 surface area in these areas in children is significantly smaller than that in adults. Some children with AH may
28 present with mouth-nasal breathing simultaneously or mouth breathing. Inspiratory airflow may enter the lower
29 respiratory tract through the mouth and may lead to additional deposition of pollen particles in the pharynx. In
30 addition, children have a far lower chance of pollen particles accessing their lower respiratory tract, compared
31 to adults. For infants, inertial impaction is the dominant deposition mechanism, thus particles are deposited
32 more in the upper airways than in the lower ([Deng et al., 2018](#)). However, more particles tend to deposited in
33 the lower airways than in the upper in adults, as gravitational sedimentation mechanism dominates ([Deng et](#)
34 [al., 2018](#)).

39 The deposition of particles in each region of the nasal cavity varies with particle diameters, breathing rates,
40 and density of particles ([Wang et al., 2009](#)). Inhaled allergen particles are transported by airflow, and for the
41 same allergen particle, changes in respiratory flow rate can significantly alter the distribution of particle
42 deposition in the nasal cavity. Studies on adults by [Inthavong et al. \(2009\)](#) and [Shi et al. \(2007\)](#) showed that
43 deposition hotspots moved forward with increasing respiratory rate and particle diameter. The deposition of
44 Artemisia pollen in this study showed consistent pattern. With increasing respiratory flow rate, about 94% of
45 the pollen was deposited in the anterior 1/3 of the nasal cavity including the nasal vestibule and the anterior
46 part of the nasal septum, with almost no particle deposition in the posterior nasal turbinate area and nasopharynx.
47 That is because under exercising conditions, the pollen can hardly follow the mainstream lines to turn due to
48 excessive particle inertia as the flow rate accelerates, and particle trajectory lines were relatively flat and
49 straight. This resulted in the direct collision of the pollens onto the nasal cavity wall. There are few reports on
50 the effect of air humidity on pollen deposition distribution. Compared to wet pollen, dry Artemisia pollen is
51 about 47 times more likely to be inhaled into the lower respiratory tract, which may put children at higher risk
52 of developing asthma. [Nastos et al. \(2008\)](#) reported that the incidence of asthma in children was higher when
53 the absolute humidity of air was low. This may be related to the increased amount of pollen dispersed in the air
54 and the longer distance it travels under dry climatic conditions, which leads to an increase in pollen inhaled
55 into the lower respiratory tract. In addition, we found large individual differences in the regional particle
56
57
58
59
60
61
62
63
64
65

deposition fractions of Artemisia pollen for the population in the same region. [Dong et al. \(2018\)](#) showed that anatomical differences in nasal vestibule morphology can significantly affect the distribution of particle deposition, while the changes of particle deposition caused by morphological differences in nasal septum, turbinate area and nasopharynx still need to be further explored.

Patient education, allergen avoidance, pharmacotherapy and allergen-specific immunotherapy are the main forms of treatment for AR. Each of these approaches is known to have its drawbacks. As the quality of people's life improves, there is a progressive demand on seeking safer, more convenient and effective alternative therapies, so nasal rinses, pollen blockers, and nasal sprays are becoming more and more prevalent in clinical practice. [Li et al. \(2013\)](#) and [Schwetz et al. \(2004\)](#) showed that the clinical symptoms of AR can be reduced by applying pollen blockers on the nasal vestibule. This is in line with the finding of this study that a great amount of Artemisia pollen is deposited in the vestibule. Furthermore, pollen deposition rates are higher in the anterior part of the nasal septum in children, which is anatomically superficial and histologically transitioned from squamous, columnar, and transitional epithelium to pseudostratified columnar epithelium. Therefore, targeted delivery of pollen blockers to this area may be more clinically significant. Based on the uniqueness of the nasal cavity and the anatomical anomalies of adenoid hypertrophy in children, in addition to the two deposition hotspots of the nasal septum and the nasal vestibule, the nasopharynx is also a major site of Artemisia pollen deposition. To better improve the therapeutic outcome, a barrier agent that can reach deep inside the nasal cavity and cover more extensive regions, such as a nasal spray, may be needed.

[Kim et al. \(2013\)](#) evaluated the dynamic growth and deposition in a child nasal airway model and reported that hygroscopic and condensation growth of water-soluble aerosols may lead to enhanced deposition. The inhaled components they studied were hygroscopic aerosols. However, our study focused on pollen particles. [Chen et al. \(2019\)](#) reported that when the relative humidity was above 90%, the increase of the mass of pollen within 200min was less than 1%. This indicates that pollen particles require an extended period to absorb moisture from the surrounding air. However, the current study suggests that the maximum travel time of inhaled pollen particles within the nasal cavity can only reach to 42.23 seconds (for one particle). While, for most particles, the travel time is considerably shorter. This timeframe is too short for pollen particles to undergo significant mass transfer with the airflow. Thus, in the current study, the hygroscopic effects were not taken into account.

Our study also has some limitations for only steady-state inspiratory states were considered, ignoring the effects of nasal cycle and nasal movement on particle deposition. Future studies should consider simulations that more closely resemble real breathing scenarios, such as the mouth-nasal dual breathing or mouth breathing modes. The current study does not cover the potential impact of aggravated allergies on nasal airway geometry, physiology, and particle deposition. However, these aspects will be investigated in our future research. Because adenoid tissue begins to degenerate when children surpass 6 years old, children over 6 years old were not included in this study and future studies could further increase the age span. In addition, comparative studies will help to elucidate the effects of individual anatomical differences and provide guidance for designing more effective drug delivery devices and pollen blocking methods.

5. Conclusions

By conducting CFD simulations, this study revealed that the deposition rates in the nasal septum and nasopharynx of children with AH were significantly higher than those of adults, whereas the deposition rates in the nasal vestibule and middle turbinate area were significantly lower, which was attributed to the uniqueness of the nasal anatomy of children. The high deposition rate in the nasopharynx may be closely related to adenoid hypertrophy. Besides individual anatomical differences, respiratory rate and pollen density were also the primary factors of deposition distribution. In addition, we established a CFD database of nasal deposition of Artemisia pollen in children with AH aged 4-6 years. Through our work, clinicians can understand the main deposition locations of Artemisia pollen in the nasal cavity of children and better guide precise application of

pollen blockers and nasal administration. The difference of deposition rate between dry and wet Artemisia pollen in nasal cavity can guide children to take appropriate allergen protection measures in dry climate.

Author contributions

Zhenzhen Hu: Conceptualization, Methodology, Validation, Formal analysis, Writing - original draft, auditing, Funding acquisition. Ruiping Ma: Conceptualization, Methodology, Formal analysis, Writing - review & editing, auditing. Yusheng Wang: Datacuration, Visualization, Supervision, Methodology. Miao Lou: Software, Validation, Investigation. Minjie Gong: Supervision, Visualization, Methodology. Botao Wang: Project administration, Validation, Methodology. Guoxi Zheng: Project administration, Supervision, Validation, Funding acquisition. Jingliang Dong: Conceptualization, Methodology, Validation, Formal analysis, Writing - review & editing, Funding acquisition. Ya Zhang: Conceptualization, Methodology, Validation, Formal analysis, Writing - review & editing, Funding acquisition.

Declaration of competing interest

The authors declare that they have no known competing financial interests or personal relationships that could have appeared to influence the work reported in this paper.

Acknowledgements

This research was funded by the National Natural Scientific Foundation of China [grant number 82000960]; the Universities Co-funded Project of Key Research and Development Project of Shaanxi Province [grant number 2020GXLH-Y-017]; the Science and Technology Planning Project of Yulin City [grant number CXY-2020-047]; and the Australian Research Council [grant number DE210101549].

References

- Anthony, T. R., Flynn, M. R., & Eisner, A. (2005). Evaluation of facial features on particle inhalation. *Annals of Occupational Hygiene*, 49(2), 179-193. <https://doi.org/10.1093/annhyg/meh082>
- Becquemin, M. H., Swift, D. L., Bouchikhi, A., Roy, M., & Teillac, A. (1991). Particle deposition and resistance in the noses of adults and children. *European Respiratory Journal*, 4(6), 694-702.
- Bennett, W. D., Zeman, K. L., & Jarabek, A. M. (2008). Nasal contribution to breathing and fine particle deposition in children versus adults. *Journal of Toxicology and Environmental Health, Part A*, 71(3), 227-237. <https://doi.org/10.1080/15287390701598200>
- Chen, L., Chen, Y., Chen, L., Gu, W., Peng, C., Luo, S., Song, W., Wang, Z., & Tang, M. (2019). Hygroscopic Properties of 11 Pollen Species in China. *ACS Earth and Space Chemistry*, 3(12), 2678-2683. <https://doi.org/10.1021/acsearthspacechem.9b00268>
- Crawford, H. J. (1949). Determination of the specific gravity of ragweed pollen (*Ambrosia elatior*) and conversion of gravity sample counts to volumetric incidence. *Public Health Reports*, 64, 1195-1200.
- Deng, Q., Ou, C., Chen, J., & Xiang, Y. (2018). Particle deposition in tracheobronchial airways of an infant, child and adult. *Science of the Total Environment*, 612, 339-346. <https://doi.org/10.1016/j.scitotenv.2017.08.240>
- Depciuch, J., Kasprzyk, I., Roga, E., & Parlinska-Wojtan, M. (2016). Analysis of morphological and molecular composition changes in allergenic *Artemisia vulgaris* L. pollen under traffic pollution using SEM and FTIR spectroscopy. *Environmental Science and Pollution Research*, 23(22), 23203-23214. <https://doi.org/10.1007/s11356-016-7554-8>

- Dogru, M., Evcimik, M. F., & Calim, O. F. (2017). Does adenoid hypertrophy affect disease severity in children with allergic rhinitis? *European Archives of Otorhinolaryngology*, 274(1), 209-213. <https://doi.org/10.1007/s00405-016-4196-x>
- Dong, J., Ma, J., Shang, Y., Inthavong, K., Qiu, D., Tu, J., & Frank-Ito, D. (2018). Detailed nanoparticle exposure analysis among human nasal cavities with distinct vestibule phenotypes. *Journal of Aerosol Science*, 121, 54- 65. <https://doi.org/10.1016/j.jaerosci.2018.05.001>
- Dong, J., Shang, Y., Inthavong, K., Tu, J., Chen, R., Bai, R., Wang, D., & Chen, C. (2016). Comparative Numerical Modeling of Inhaled Nanoparticle Deposition in Human and Rat Nasal Cavities. *Toxicological Sciences*, 152(2), 284-296. <https://doi.org/10.1093/toxsci/kfw087>
- Dong, J., Shang, Y., Tian, L., Inthavong, K., Qiu, D., & Tu, J. (2019). Ultrafine particle deposition in a realistic human airway at multiple inhalation scenarios. *International journal for numerical methods in biomedical engineering*, 35(7). <https://doi.org/10.1002/cnm.3215>. Article e3215
- Dong, J., Sun, Q., Shang, Y., Zhang, Y., Tian, L., & Tu, J. (2022). Numerical comparison of inspiratory airflow patterns in human nasal cavities with distinct age differences. *International journal for numerical methods in biomedical engineering*, 38(3). <https://doi.org/10.1002/cnm.3565>. Article e3565
- Elwany, S. (1987). The adenoidal-nasopharyngeal ratio (AN ratio). Its validity in selecting children for adenoidectomy. *The Journal of Laryngology and Otology*, 101(6), 569-573. <https://doi.org/10.1017/s0022215100102269>
- Evcimik, M. F., Dogru, M., Cirik, A. A., & Nepesov, M. I. (2015). Adenoid hypertrophy in children with allergic disease and influential factors. *International Journal of Pediatric Otorhinolaryngology*, 79(5), 694-697. <https://doi.org/10.1016/j.ijporl.2015.02.017>
- Farhadi, G. P., Keshavarzian, E., Abouali, O., Faramarzi, A., Tu, J., & Shakibafard, A. (2012). Numerical analysis of micro- and nano-particle deposition in a realistic human upper airway. *Computers in Biology and Medicine*, 42(1), 39-49. <https://doi.org/10.1016/j.combiomed.2011.10.005>
- Fujioka, M., Young, L. W., & Girdany, B. R. (1979). Radiographic evaluation of adenoidal size in children: adenoidal-nasopharyngeal ratio. *AJR American Journal of Roentgenology*, 133(3), 401-404. <https://doi.org/10.2214/ajr.133.3.401>
- Garcia, G. J., Schroeter, J. D., & Kimbell, J. S. (2015). Olfactory deposition of inhaled nanoparticles in humans. *Inhalation toxicology*, 27(8), 394-403. <https://doi.org/10.3109/08958378.2015.1066904>
- Golshahi, L., Noga, M. L., Thompson, R.B., & Finlay, W. H. (2011). In vitro deposition measurement of inhaled micrometer-sized particles in extrathoracic airways of children and adolescents during nose breathing. *Journal of Aerosol Science*, 42(7), 474-488. <https://doi.org/10.1016/j.jaerosci.2011.04.002>
- Golshahi, L., & Hosseini, S. (2019). Intranasal Filtration of Inhaled Aerosol in Human Subjects as a Function of Nasal Pressure Drop. *Journal of Aerosol Medicine and Pulmonary Drug Delivery*, 32(1), 13-23. <https://doi.org/10.1089/jamp.2018.1476>
- Hazeri, M., Faramarzi, M., Sadrizadeh, S., Ahmadi, G., & Abouali, O. (2021). Regional deposition of the allergens and micro-aerosols in the healthy human nasal airways. *Journal of Aerosol Science*, 152. <https://doi.org/10.1016/j.jaerosci.2020.105700>. Article 105700
- Hofmann, W. (1982). Mathematical model for the postnatal growth of the human lung. *Respiration Physiology*, 49(1), 115-129. [https://doi.org/10.1016/0034-5687\(82\)90106-2](https://doi.org/10.1016/0034-5687(82)90106-2)
- Huang, S. W., & Giannoni, C. (2001). The risk of adenoid hypertrophy in children with allergic rhinitis. *Annals of Allergy, Asthma, & Immunology*, 87(4), 350-355. [https://doi.org/10.1016/S1081-1206\(10\)62251-X](https://doi.org/10.1016/S1081-1206(10)62251-X)
- Inthavong, K., Shang, Y., Del, G. J., Wise, S. K., Edwards, T. S., Bradshaw, K., Wong, E., Smith, M., & Singh, N. (2021). Inhalation and deposition of spherical and pollen particles after middle turbinate resection in a

- human nasal cavity. *Respiratory Physiology & Neurobiology*, 294. <https://doi.org/10.1016/j.resp.2021.103769>. Article 103769
- Inthavong, K., Tu, J., & Goodarz, A. (2009). Computational Modelling of Gas-Particle Flows with Different Particle Morphology in the Human Nasal Cavity. *The Journal of Computational Multiphase Flows*, 1(1), 57-82. <https://doi.org/10.1260/175748209787387061>
- Inthavong, K., Wen, J., Tu, J., & Tian, Z. (2009). From CT Scans to CFD Modelling – Fluid and Heat Transfer in a Realistic Human Nasal Cavity. *Engineering Applications of Computational Fluid Mechanics*, 3(3), 321-335. <https://doi.org/10.1080/19942060.2009.11015274>
- Izquierdo-Dominguez, A., Jauregui, I., Del, C. A., Montoro, J., Davila, I., Sastre, J., Bartra, J., Ferrer, M., Alobid, I., Mullol, J., & Valero, A. L. (2017). Allergy rhinitis: similarities and differences between children and adults. *Rhinology*, 55(4), 326-331. <https://doi.org/10.4193/Rhino17.074>
- Izquierdo-Dominguez, A., Valero, A. L., & Mullol, J. (2013). Comparative analysis of allergic rhinitis in children and adults. *Current Allergy and Asthma Reports*, 13(2), 142-151. <https://doi.org/10.1007/s11882-012-0331-y>
- James, B. H., & Kurt, M. (1963). Ragweed Pollen Density. *American Journal of Botany*, 50(6), 532- 539.
- Kim, J. W., Xi, J., & Si, X. A. (2013). Dynamic growth and deposition of hygroscopic aerosols in the nasal airway of a 5-year-old child. *International Journal for Numerical Methods in Biomedical Engineering*, 29(1), 17-39. <https://doi.org/10.1002/cnm.2490>
- Li, Y., Wang, D., Liu, Q., & Liu, J. (2013). Randomized double-blind placebo-controlled crossover study of efficacy of pollen blocker cream for perennial allergic rhinitis. *American Journal of Rhinology & Allergy*, 27(4), 299-303. <https://doi.org/10.2500/ajra.2013.27.3923>
- Lou, Z. (2018). Adenoid hypertrophy in children and allergic rhinitis. *European Archives of Otorhinolaryngology*, 275(3), 831-832. <https://doi.org/10.1007/s00405-017-4737-y>
- Marcus, C. L., Brooks, L. J., Draper, K. A., Gozal, D., Halbower, A. C., Jones, J., Schechter, M. S., Sheldon, S. H., Spruyt, K., Ward, S. D., Lehmann, C., & Shiffman, R. N. (2012). Diagnosis and management of childhood obstructive sleep apnea syndrome. *Pediatrics*, 130(3), 576-584. <https://doi.org/10.1542/peds.2012-1671>
- Modrzynski, M., & Zawisza, E. (2007a). The influence of birch pollination on the adenoid size in children with intermittent allergic rhinitis. *International Journal of Pediatric Otorhinolaryngology*, 71(7), 1017-1023. <https://doi.org/10.1016/j.ijporl.2007.02.018>
- Modrzynski, M., & Zawisza, E. (2007b). An analysis of the incidence of adenoid hypertrophy in allergic children. *International Journal of Pediatric Otorhinolaryngology*, 71(5), 713-719. <https://doi.org/10.1016/j.ijporl.2006.12.018>
- Moideen, S. P., Mytheenkunju, R., Govindan, N. A., Mogarnad, M., & Afroze, M. (2019). Role of Adenoid-Nasopharyngeal Ratio in Assessing Adenoid Hypertrophy. *Indian Journal of Otolaryngology and Head & Neck Surgery*, 71, 469-473. <https://doi.org/10.1007/s12070-018-1359-7>
- Moreddu, E., Meister, L., Philip-Alliez, C., Triglia, J. M., Medale, M., & Nicollas, R. (2019). Computational Fluid Dynamics in the assessment of nasal obstruction in children. *European Annals of Otorhinolaryngology, Head and Neck diseases*, 136(2), 87-92. <https://doi.org/10.1016/j.anorl.2018.11.00>
- Nastos, P. T., Paliatsos, A. G., Papadopoulos, M., Bakoula, C., & Priftis, K. N. (2008). The effect of weather variability on pediatric asthma admissions in Athens, Greece. *Journal of Asthma*, 45(1), 59-65. <https://doi.org/10.1080/02770900701815818>
- Ohsaki, S., Mitani, R., Fujiwara, S., Nakamura, H., & Watano, S. (2019). Effect of Particle-Wall Interaction and Particle Shape on Particle Deposition Behavior in Human Respiratory System. *Chem Pharm Bull*

(Tokyo), 67(12), 1328-1336. <https://doi.org/10.1248/cpb.c19-00693>

- Ounis, H., Ahmadi, G., & McLaughlin, J. B. (1991). Brownian diffusion of submicrometer particles in the viscous sublayer. *Journal of Colloid and Interface Science*, 143(1), 266-277. [https://doi.org/10.1016/0021-9797\(91\)90458-K](https://doi.org/10.1016/0021-9797(91)90458-K)
- Pereira, L., Monyror, J., Almeida, F. T., Almeida, F. R., Guerra, E., Flores-Mir, C., & Pacheco-Pereira, C. (2018). Prevalence of adenoid hypertrophy: A systematic review and meta-analysis. *Sleep Medicine Reviews*, 38, 101-112. <https://doi.org/10.1016/j.smrv.2017.06.001>
- Schwetz, S., Olze, H., Melchisedech, S., Grigorov, A., & Latza, R. (2004). Efficacy of pollen blocker cream in the treatment of allergic rhinitis. *Archives of Otolaryngology -- Head and Neck Surgery*, 130(8), 979-984. <https://doi.org/10.1001/archotol.130.8.979>
- Shang, Y., Inthavong, K., & Tu, J. (2015). Detailed micro-particle deposition patterns in the human nasal cavity influenced by the breathing zone. *Computers and Fluids*, 114, 141-150. <https://doi.org/10.1016/j.compfluid.2015.02.020>
- Shi, H., Kleinstreuer, C., & Zhang, Z. (2007). Modeling of inertial particle transport and deposition in human nasal cavities with wall roughness. *Journal of Aerosol Science*, 38(4), 398-419. <https://doi.org/10.1016/j.jaerosci.2007.02.002>
- Simantirakis, G., Hourdakakis, C. J., Economides, S., & Dimitriou, P. (2011). Image quality and patient dose in computed tomography examinations in Greece. *Radiation Protection Dosimetry*, 147(1-2), 129-132. <https://doi.org/10.1093/rpd/ncr282>
- Sun, Q., Dong, J., Zhang, Y., Tian, L., & Tu, J. (2022). Numerical study of the effect of nasopharynx airway obstruction on the transport and deposition of nanoparticles in nasal airways. *Experimental and Computational Multiphase Flow*, 4(4), 399-408. <https://doi.org/10.1007/s42757-022-0143-9>
- Thiriet, M. (2014). *Biomathematical and Biomechanical Modeling of the Circulatory and Ventilatory Systems*. New York: Springer.
- Tian, L., Shang, Y., Chen, R., Bai, R., Chen, C., Inthavong, K., & Tu, J. (2019). Correlation of regional deposition dosage for inhaled nanoparticles in human and rat olfactory. *Particle and Fibre Toxicology*, 16(1), 6. <https://doi.org/10.1186/s12989-019-0290-8>
- Wang, S. M., Inthavong, K., Wen, J., Tu, J. Y., & Xue, C. L. (2009). Comparison of micron- and nanoparticle deposition patterns in a realistic human nasal cavity. *Respiratory Physiology & Neurobiology*, 166(3), 142-151. <https://doi.org/10.1016/j.resp.2009.02.014>
- Xi, J., Kim, J., Si, X. A., Su, W. C., & Zhou, Y. (2014b). Effects of the facial interface on inhalation and deposition of micrometer particles in calm air in a child airway model. *Inhalation toxicology*, 26(8), 492-505. <https://doi.org/10.3109/08958378.2014.925992>
- Xi, J., Si, X., Won, J. M., & Berlinski, A. (2011). Simulation of airflow and aerosol deposition in the nasal cavity of a 5- year- old child. *Journal of Aerosol Science*, 42, 156- 173. <https://doi.org/10.1016/j.jaerosci.2010.12.004>
- Xi, J., Si, X., Zhou, Y., Kim, J., & Berlinski, A. (2014a). Growth of nasal and laryngeal airways in children: implications in breathing and inhaled aerosol dynamics. *Respiratory Care*, 59(2), 263-273. <https://doi.org/10.4187/respcare.02568>
- Zhang, Y., Shang, Y., Inthavong, K., Tong, Z., Sun, B., Zhu, K., Yu, A., & Zheng, G. (2019). Computational investigation of dust mite allergens in a realistic human nasal cavity. *Inhalation toxicology*, 31(6), 224-235. <https://doi.org/10.1080/08958378.2019.1647315>
- Zhang, Y., Zhang, L., Huang, F., Zhang, J., Lou, M., Sun, B., Zhu, K., Zheng, G., & Tong, Z. (2019). Computational investigation of Artemisia pollen deposition in realistic nasal cavities of residents in northwest China. *Chinese Journal of Otorhinolaryngology Head and Neck Surgery*, 54(10), 741-747.

Zhou, Y., Xi, J., Simpson, J., Irshad, H., & Cheng, Y. (2013). Aerosol Deposition in a Nasopharyngolaryngeal Replica of a 5-Year-Old Child. *Aerosol Science and Technology*, 47(3), 275-282. <https://doi.org/10.1080/02786826.2012.749341>

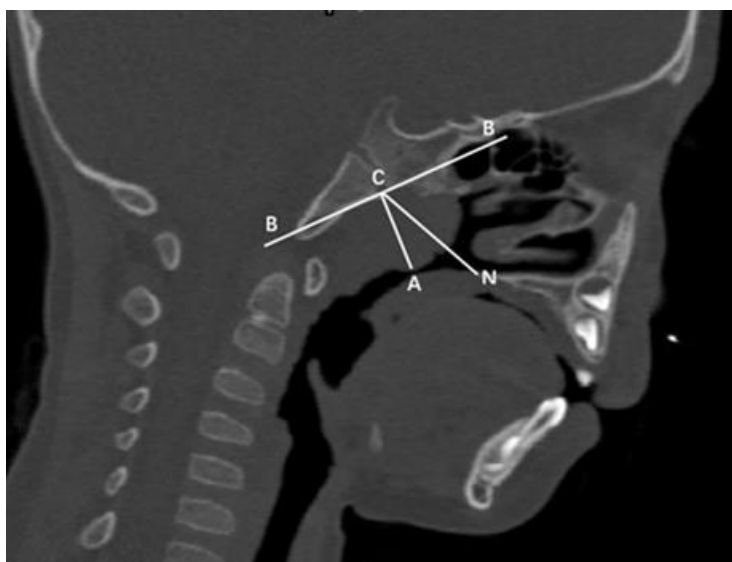


Fig.1. Method of calculating the adenoidal-nasopharyngeal (AN) ratio based on CT images. BB: Line drawn along the straight part of the anterior margin of the basiocciput; AC: Adenoid thickness (perpendicular distance from the outermost point of convexity of the adenoid shadow to BB); NC: Nasopharyngeal width (distance from the posterior end of the hard palate or the superior edge of the anterior middle area of the soft palate to the anteroinferior edge of the sphenoccipital synchondrosis); AN ratio calculated by dividing AC with NC.

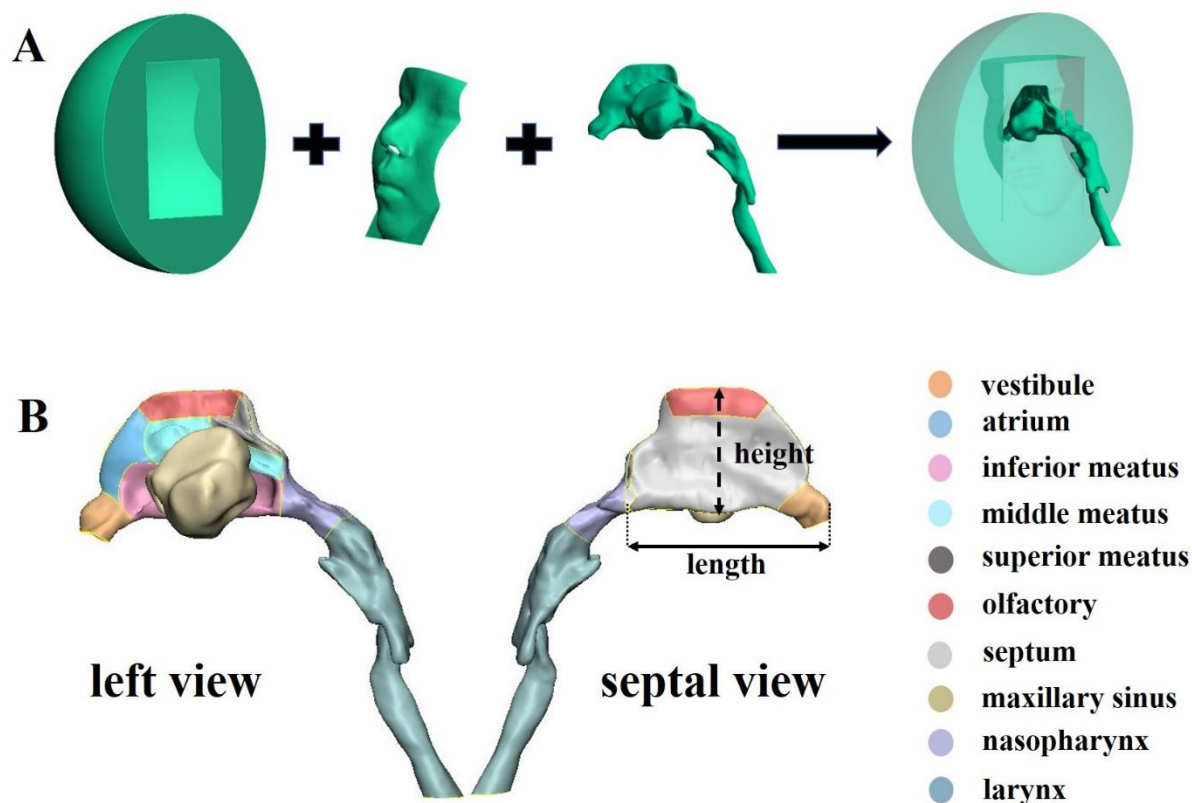


Fig. 2. Three-dimensional (3D) model of nasal cavity and paranasal sinus and its regional division. (A) 3D model of nasal cavity and paranasal sinus. (B) regional division of nasal cavity (the solid black line indicates the length of the nasal cavity and the dashed black line indicates the height of the nasal cavity).

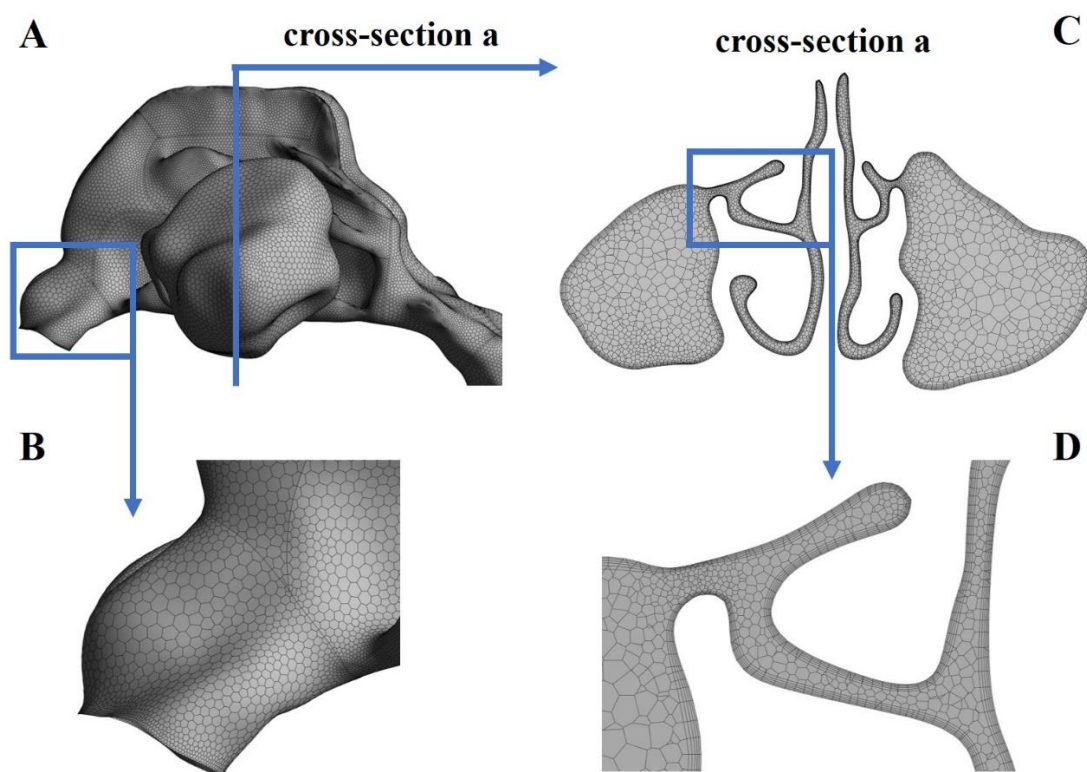


Fig. 3. Polyhedral mesh of nasal cavity and cross section. (AB) the surface mesh. (CD) the volume mesh on a cross-section.

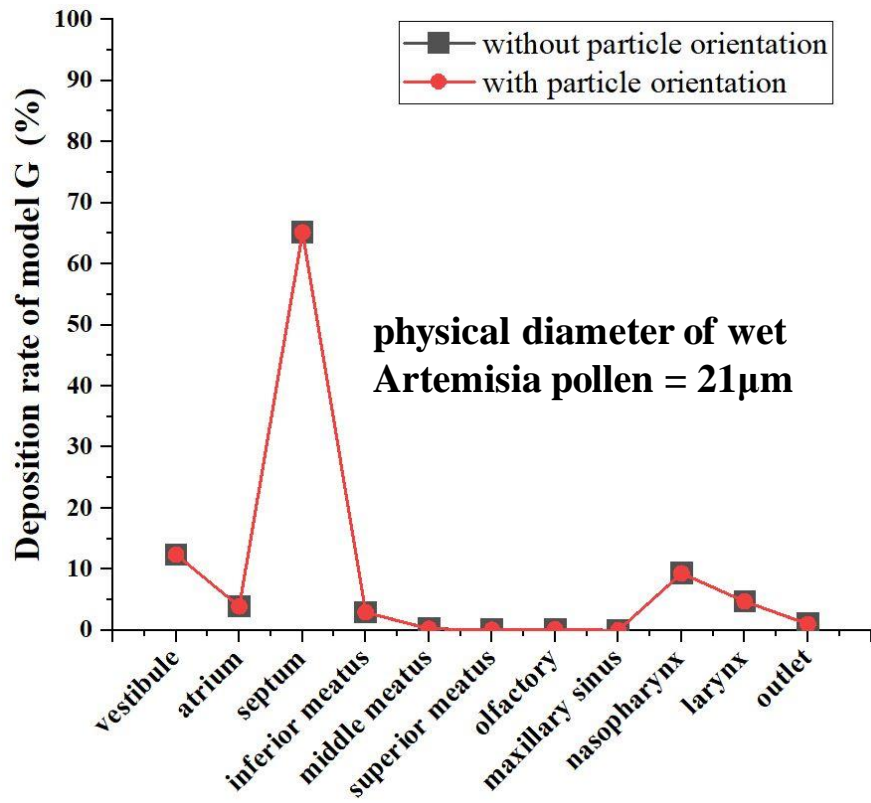


Fig. 4. For wet Artemisia pollen with a physical diameter of 21µm, comparison of simulation results for model G considering and not considering particle orientation.

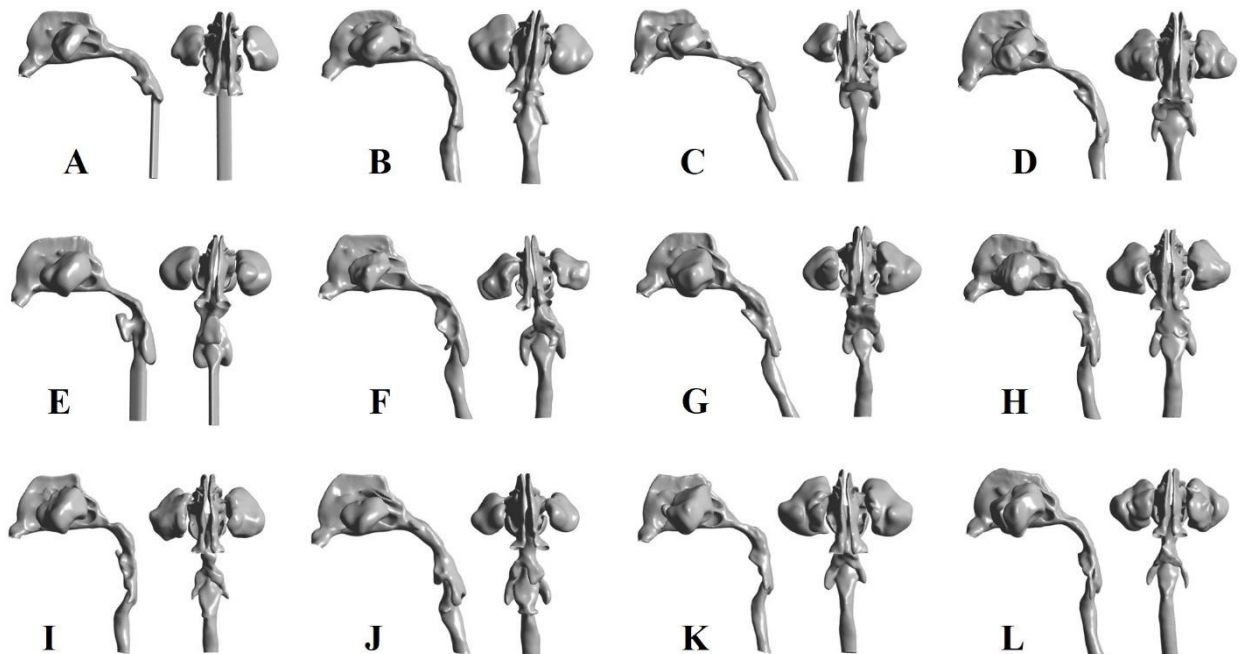


Fig. 5. 3D geometry of the upper airway of the children in this study.

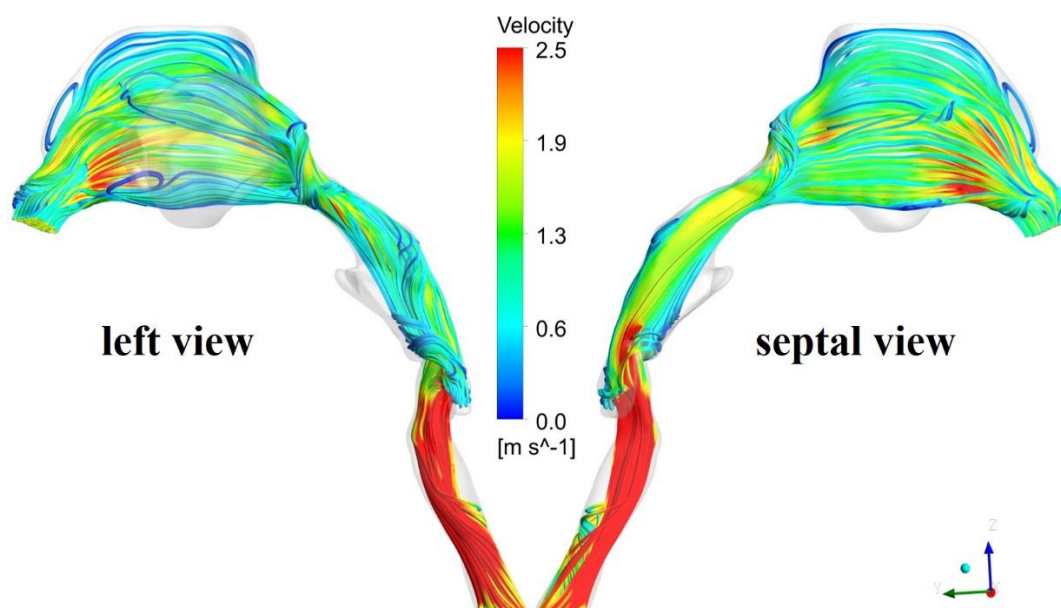


Fig. 6. Airflow streamlines in the nasal cavity of children in resting state.

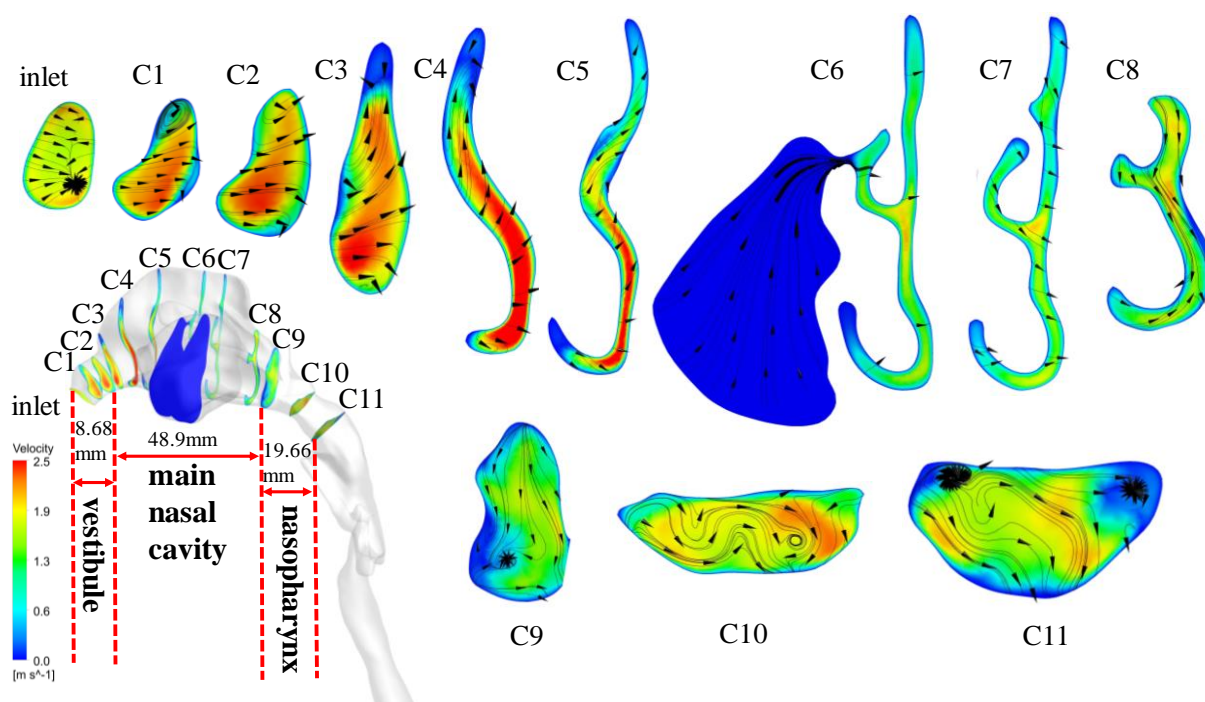


Fig. 7. Axial flow and secondary flow model diagrams at each characteristic cross-section in resting state. The red double arrows represent the horizontal length of the nasal vestibule, main nasal cavity, and nasopharynx.

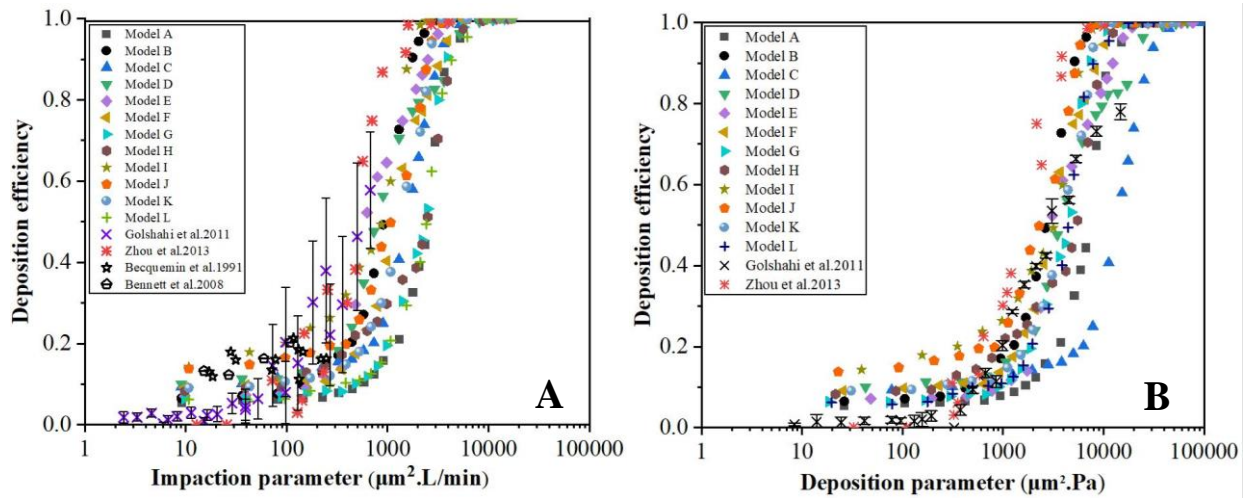


Fig. 8. (A) Deposition efficiency of the pediatric nasal model as a function of impactation parameter, compared with the deposition data in the literature. (B) Deposition efficiency of the pediatric nasal model as a function of particle size and pressure drop, compared with the deposition data in the literature.

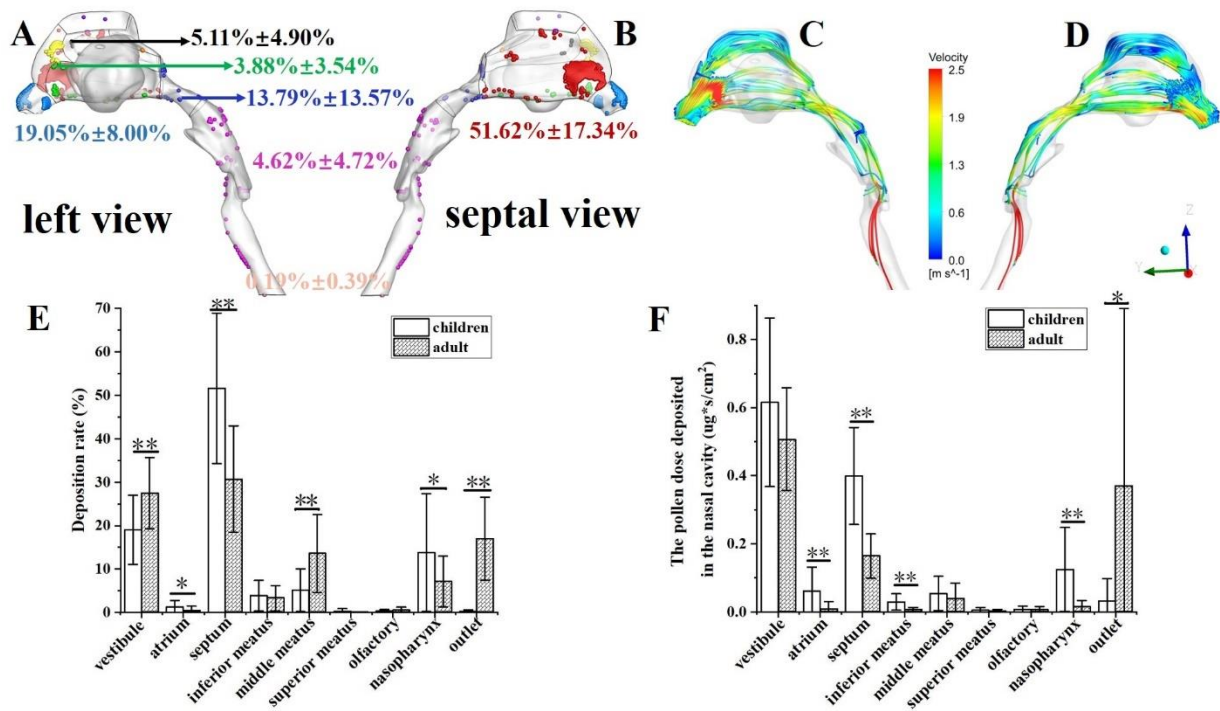


Fig. 9. (AB) Deposition diagram of wet Artemisia pollen in nasal cavity in resting state. (CD) Particle trajectories of wet Artemisia pollen in nasal cavity in resting state. (E) Deposition rate in each anatomical site and escape rate from outlet of wet Artemisia pollen among children and healthy adults (** indicates $p < 0.01$, * indicates $p < 0.05$). (F) Deposition dose of wet Artemisia pollen at various anatomical sites in children and healthy adults (** indicates $p < 0.01$, * indicates $p < 0.05$). Regional doses information was calculated based on 1 second.

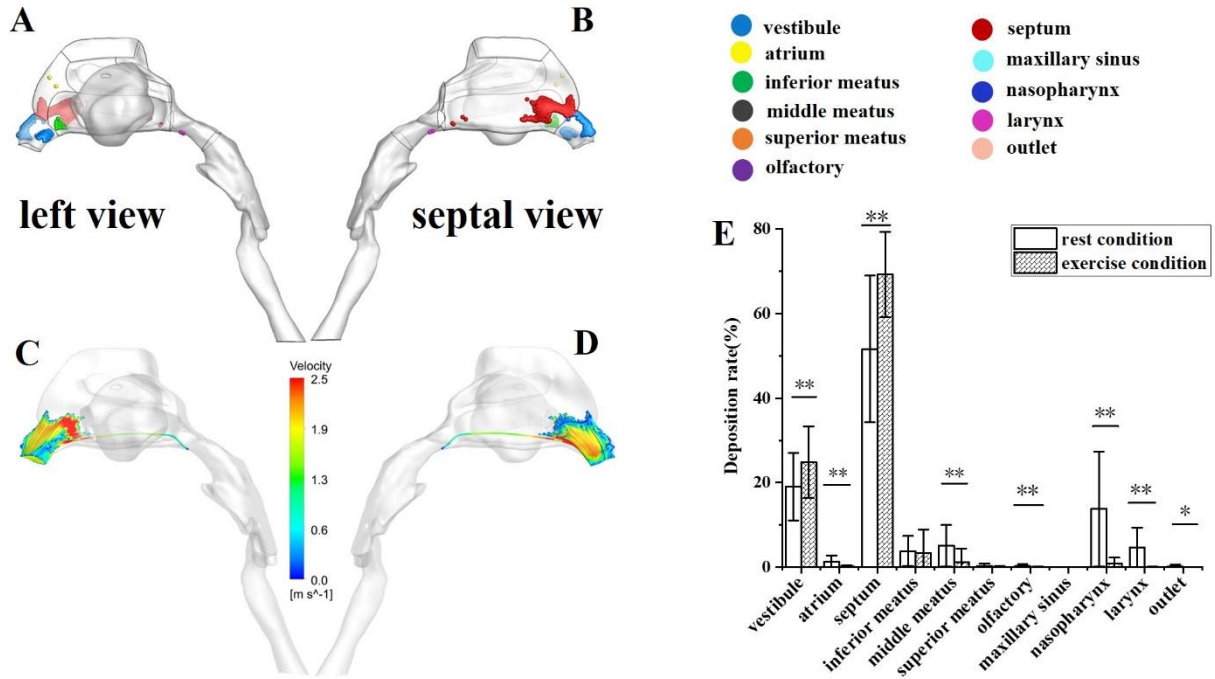


Fig. 10. (AB) Deposition diagram of wet Artemisia pollen in nasal cavity in exercising state. (CD) Particle trajectories of wet Artemisia pollen in nasal cavity in exercising state. (E) Deposition rate in each anatomical site and escape rate from outlet of wet Artemisia pollen under different inspiratory flow rates (** indicates $p<0.01$, * indicates $p<0.05$).

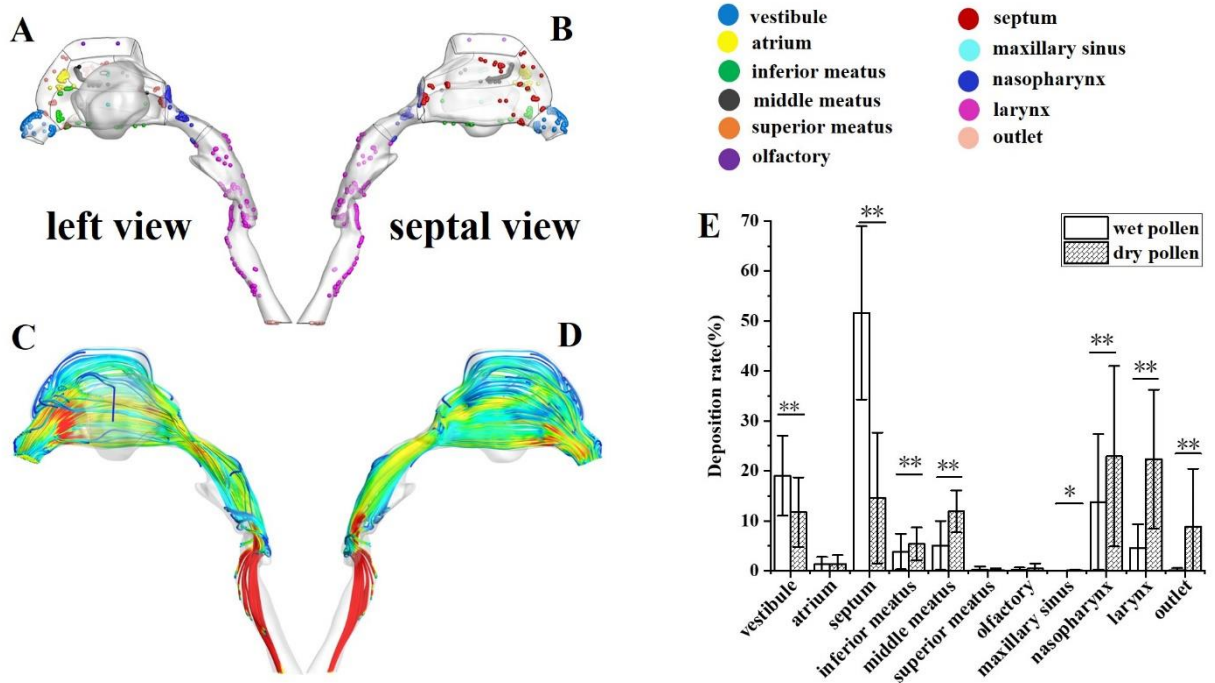


Fig. 11. (AB) Deposition diagram of dry Artemisia pollen in nasal cavity in resting state. (CD) Particle trajectories of dry Artemisia pollen in nasal cavity in resting state. (E) Deposition rate in each anatomical site and escape rate from outlet of wet and dry Artemisia pollen in nasal cavities of children (** indicates $p<0.01$, * indicates $p<0.05$).

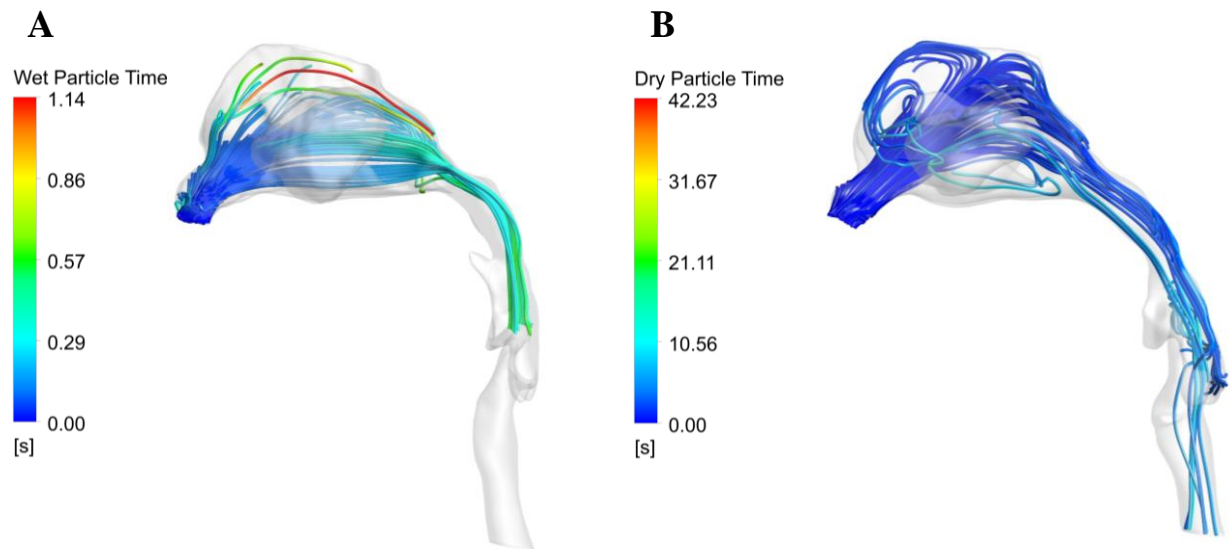

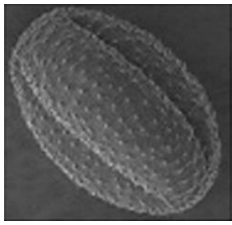


Fig. 12. (A) Particle trajectories coloured by transport time for wet pollen in representative model H. (B) Particle trajectories coloured by transport time for dry pollen in representative model J.

Table 1
Shapes images of *Artemisia* pollen.

Shape		Density	SEM image	Shape factor
Ellipsoid	2a=22.1µm	Wet pollen 840-1320 kg/m ³		0.99
	2b=20.6µm	Dry pollen 550 kg/m ³		

SEM (scanning electron microscope), image sourced from [Depciuch et al. \(2016\)](#).

Table 2

Deposition data of wet Artemisia pollen in children models.

Anatomic partition	Deposition rate (%)	surface area (cm ²)	Deposition dose (µg*s/cm ²)
Vestibule	19.05±8.00	3.20±0.48	0.6153±0.2475
Atrium	1.30±1.50	2.25±0.25	0.0605±0.0706
Septum	51.62±17.34	13.57±1.43	0.3994±0.1424
Inferior meatus	3.88±3.54	13.62±1.72	0.0292±0.0243
Middle meatus	5.11±4.90	9.84±1.76	0.0543±0.0503
Superior meatus	0.25±0.65	2.51±0.64	0.0048±0.0082
Olfactory	0.31±0.39	4.70±0.70	0.0074±0.0097
Maxillary sinuses	0.01±0.02	21.25±4.69	0.00003±0.0001
Nasopharynx	13.79±13.57	11.69±1.49	0.1246±0.1232
Larynx	4.62±4.72	31.39±7.90	0.0157±0.0162
Outlet	0.19±0.39	0.70±0.21	0.0317±0.0664

Table 3

Deposition data of wet Artemisia pollen in adult models.

Anatomic partition	Deposition rate (%)	surface area (cm ²)	Deposition dose (µg*s/cm ²)
Vestibule	27.45±8.21	5.25±1.08	0.5072±0.1509
Atrium	0.40±1.09	3.70±0.63	0.0082±0.0221
Septum	30.70±12.27	21.19±2.53	0.1641±0.0650
Inferior meatus	3.30±2.90	26.55±4.35	0.0068±0.0064
Middle meatus	13.59±8.98	20.27±2.41	0.0390±0.0455
Superior meatus	0.05±0.12	1.74±0.35	0.0021±0.0053
Olfactory	0.46±0.78	6.28±1.18	0.0059±0.0100
Nasopharynx	7.14±5.90	24.10±5.59	0.0147±0.0191
Outlet	17.00±9.57	1.62±0.44	0.3709±0.5477

Highlights

- Quantitative studies of particle deposition were performed in the largest cohort of children with adenoid hypertrophy to date.
- The interaction among nasal anatomy, airflow and particles is described qualitatively and quantitatively.
- The geometric features of the nasal cavity in children aged 4-6 years were quantified.
- The correlation between deposition hotspots and allergic symptoms in children was revealed.
- A database of Artemisia pollen deposition in the upper airway of children with adenoid hypertrophy was established.